

# Time-Frequency Characterization of Micro-Multipath Signals in Over-the-Horizon Radar

Cornel Ioana<sup>1</sup>, Yimin D. Zhang<sup>2</sup>, Moeness G. Amin<sup>2</sup>, Fauzia Ahmad<sup>2</sup>, Gordon Frazer<sup>3</sup>, Braham Himed<sup>4</sup>

<sup>1</sup> Grenoble Institute of Technology, GIPSA-lab, Signal-Image Department, Saint Martin d'Hères, France

<sup>2</sup> Center for Advanced Communications, Villanova University, Villanova, PA 19085, USA

<sup>3</sup> Intelligence, Surveillance and Reconnaissance Division, Defence Science and Technology Organisation, Australia

<sup>4</sup> Air Force Research Laboratory, AFRL/RVMD, Dayton, OH 4543, USA

**Abstract** — A challenging task in over-the-horizon radar (OTHR) is the tracking of target altitude. It has been shown that the micro-multipaths due to ocean/ground reflections may reveal important information about the elevation maneuvering of a target. The Doppler signature of such micro-multipath signals is typically composed of three components having close nonlinear time-frequency behaviors. In this paper, we develop novel time-frequency analysis techniques for the characterization of Doppler effect of micro-multipath signals. The proposed method is based on the local analysis of the signal phase, followed by a stationarization operator. In the warped representation domain, the multi-component nonlinear Doppler signatures become stationary, thus allowing the application of spectral analysis tools. The results presented are based on real data and illustrate the potential of the proposed methods.

## I. INTRODUCTION

Over-the-horizon radar (OTHR) systems serve as a critical technology in national defense and homeland security. An OTHR performs a wide-area surveillance at long range that is well beyond the limit of the horizon of conventional line-of-sight (LOS) radars. An important yet challenging task in OTHR systems is the accurate geolocation estimation of maneuvering targets. In particular, the altitude of a maneuvering target is critical for its tracking and classification. Since OTHR systems employ narrowband signals, direct estimation of target altitude is infeasible. A practical and tangible method for providing the altitude information can be based on micro-multipath model that makes use of multipath returns due to the ocean or ground reflections local to the target [1]. The micro-multipath returns of a maneuvering target yield multiple Doppler signatures that are typically very closely separated and cannot be resolved in range. These returns, however, manifest themselves as different nonlinear time-frequency trajectories, each corresponds to a Doppler signature of the target along a propagation path. It has been shown in [2] that high-resolution time-frequency analysis of the Doppler signatures

can resolve Doppler signatures, enabling fast and robust altitude tracking. However, the similarities of the Doppler signatures and the nature of their nonstationarities, together with artifacts corresponding to the clutter require further analytical and algorithmic developments.

This paper presents novel time-frequency analysis techniques that provide improved multi-component nonlinear Doppler signature estimation. In particular, we develop a method that is based on the local analysis of the signal phase, followed by conversion to stationarity and approximately to fixed-frequency sinusoids. This conversion enables the application of both parametric and nonparametric signal analysis methods. The estimated fixed frequencies are transformed via the inverse frequency operator, leading to the resolved time-frequency trajectories, or the Doppler signatures, of the propagation paths.

The paper is structured as follows. Section II reviews the concept of utilizing multi-component Doppler signatures for the altitude tracking of a maneuvering target. The measured maneuvering scene is described in Section III. The local analysis and global fusion of the phase information will be described in Section IV. The results generated using measured real data, illustrated in Section V, highlight the potential of the proposed method.

## II. ALTITUDE TRACKING OF MANEUVERING TARGET

As shown in Fig. 1, the local multipath around a target, due to ground/ocean reflections, yields different propagation paths of the emitted/received signals which, in turn, result in the following three combinations. The first and second components correspond to both the emitted and received signals propagating along path I and path II, respectively. The third component is a result of the emitted signal traveling along path I and the received signal propagating along path II or vice versa. In Fig. 1,  $H$  is the height of the ionosphere layer, and  $h$  is the height of the target.

Under this assumption, the received signal can be expressed as follows:

$$x(t) = A_1 e^{j\varphi_1(t)} + A_2 e^{j\varphi_2(t)} + A_3 e^{j\varphi_3(t)}, \quad (1)$$

where  $A_1$ ,  $A_2$  and  $A_3$  are the path losses, and  $\{\varphi_i\}$ 's are the instantaneous phase laws. Invoking the flat-earth ionosphere

---

The work of Y. D. Zhang, M. G. Amin, and F. Ahmad is supported in part by a subcontract with Dynetics, Inc. for research sponsored by the Air Force Research Laboratory (AFRL) under Contract FA8650-08-D-1303.

mirror model and assuming that  $R \gg H \gg h$ , where  $R$  is the ground range, the three phase laws can be expressed as [2]

$$\begin{aligned}\varphi_1(t) &= -\frac{4\pi f_c}{c} \int \left[ K(t)v_R(t) - \frac{2H}{R(t)}v_c(t) \right] dt \\ \varphi_2(t) &= -\frac{4\pi f_c}{c} \int \left[ K(t)v_R(t) + \frac{2H}{R(t)}v_c(t) \right] dt \\ \varphi_3(t) &= -\frac{4\pi f_c}{c} \int K(t)v_R(t) dt\end{aligned}\quad (2)$$

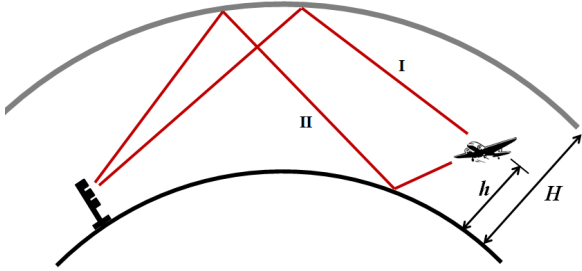


Figure 1. Definition of the propagation paths in the OTHR.

In eq. (2),  $K(t) = (1 - 2H^2/R^2(t))$ ,  $v_R(t) = dR(t)/dt$  is the target velocity in the range direction, and  $v_c(t) = dh(t)/dt$  is the velocity of the target along the vertical position. Therefore, it is clear that the elevation velocity of the maneuvering target can be tracked by estimating the difference of the Doppler signature between the three paths.

### III. DESCRIPTION OF MANEUVERING SCENE

The signals considered in this paper are real measurement data obtained by Australian Defence Science and Technology Organisation (DSTO) that consist of return waveforms received from a maneuvering plane. The data sets contain a period of 181 seconds of data collected in April 2003. The corresponding maneuvering trajectory is shown in Fig. 2 on a Google Earth view. An aircraft descends its altitude by approximately 2500 meters while making a 360° turn.

In the measured data set, the transmit and receive antenna arrays are located on land separated by approximately 100 km. The surface range between the radar site and the target is approximately 1350 km. The carrier frequency is 16 MHz, and the pulse repetition frequency (PRF) is 40 Hz. There are 256 sweeps per dwell and each dwell has a 2 sweep “inter-dwell” gap.

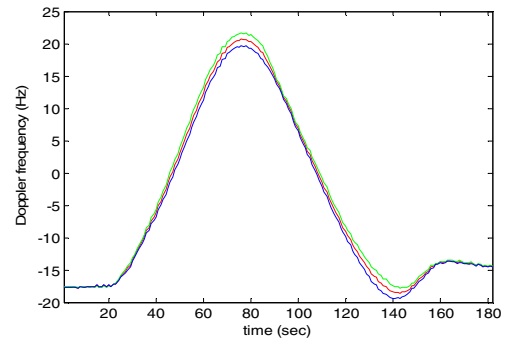
To facilitate signal processing, we first filter out the clutter in the data set by rejecting all the signals within a narrow lowpass frequency band. Phase information across different dwells is manually aligned to allow coherent signal processing over multiple dwells.

Fig. 3(a) shows the corresponding multi-component Doppler signatures estimated from the recorded GPS positions of the maneuvering target, whereas the spectrogram

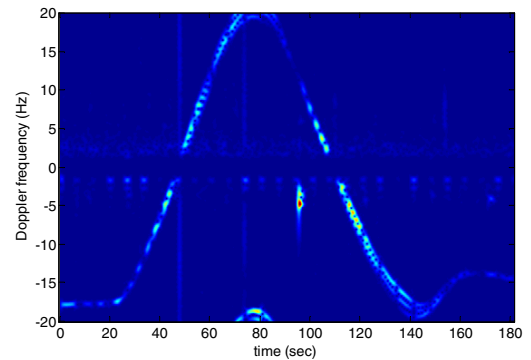
of the measured and lowpass filtered data is shown in Fig. 3(b) for comparison. The window size used in computing the spectrogram is 512 samples (12.8 seconds). Note that Doppler frequency components higher than 20 Hz are aliased into the negative frequency region in Fig. 3(b) due to the PRF limitation.



Figure 2. Google Earth view of the aircraft's trajectory.



(a) Estimated from GPS locations of the target



(b) Spectrogram of the measured data

Figure 3. Multi-component Doppler signatures.

### IV. TIME-FREQUENCY ANALYSIS

A step-by-step illustration of the proposed time-frequency analysis technique is shown in Fig. 4. A coarse estimation of the overall time-frequency signature is first obtained. This estimation is used for global time-frequency filtering and linearization of the Doppler signature through warping. The resulting Doppler signatures, which are approximately linear, allow convenient spectral analysis and estimation. The

original Doppler signatures can be recovered by inversely warping the estimated spectrum. The key steps are detailed below.

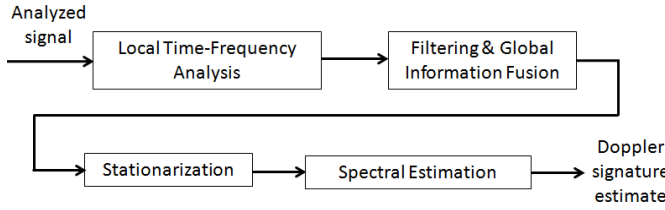


Figure 4. Proposed processing diagram of the OTHR signals

#### A. Local Time-Frequency Analysis

Time-frequency analysis is a powerful tool to analyze non-stationary signals. In the widely and commonly used Cohen's class [3], time-frequency distributions can be constructed by appropriately weighting the ambiguity domain of a signal to tradeoff the energy concentration and cross-term interference reduction. According to the kernels used for the weighting, different distributions have been defined.

Local analyses of time-frequency signatures have been studied in the context of the OTHR in [4]. The primary challenges lie in the difficulty of identifying the closely spaced target time-frequency components in the presence of residual clutter power as well as various types of noise (e.g., impulsive noise). We have examined a number of time-frequency analysis techniques and concluded that, without proper time-frequency association as described below, these techniques fail to consistently identify the true Doppler signature.

The proposed technique is based on the local analysis of time, frequency, and phase coherence, and uses this information to merge local components so as to estimate the global time-frequency structures characterizing the signal. The results are followed by warping the signal so that the Doppler signatures are filtered and stationarized, thus allowing the application of spectral analysis tools for accurate estimation of the multi-component Doppler signatures. As the signal is characterized by nonlinear heterogeneous time-frequency components, its short-time analysis is a natural way to represent *efficiently* the time-frequency content of the signal.

In this paper, the short-time polynomial phase modeling of order 2 is used and applied by warped high-order ambiguity function (WHAF) [4]. This analysis is performed over half-overlapped adjacent windows. For each window position, the WHAF yields the second-order phase modeling of the components. In real situations, this modeling is approximate and is affected by noise and close proximity of the different Doppler components. For this reason, WHAF provides, for each window, several possible estimates of the same component. Among these estimates, only one will emerge to be most appropriate, as we will discuss in step B. Assume that  $N_c$  estimates are obtained for each window corresponding to a Doppler component, and denote the set of phase functions obtained from WHAF-based phase modeling

applied in the  $i$ th window as

$$D^{(i)} = \{\psi_k^{(i)}\}_{k=1, \dots, N_c} \quad (3)$$

where  $\psi_k^{(i)}$  is the  $k$ th phase function of order 2, defined as

$$\psi_k^{(i)}(t) = \sum_{i=1}^2 a_{ki} t^i; t \in [iT; (i+3/2)T] \quad (4)$$

and  $T$  is the window size.

The second-order modeling is more robust in a noisy condition and, therefore, is more preferred than the third-order modeling [5]. Because clutter components are concentrated in low frequencies, the chirps approximating these components will have small values of the chirp rates (coefficients  $a_{k2}$  in eq. (4)).

#### B. Filtering & Global Information Fusion

The phase functions described in eq. (4) are merely an approximation of the real time-frequency content of the signal. For this reason, they are used for regrouping procedure provided in the second step of the proposed method – *fusion of local time-frequency-phase information*. The phase functions in eq. (4) are used to build local filter functions which extract the signal's samples corresponding to the time-frequency regions defined in the neighborhood of the local functions.

Let us consider signal  $x(t)$  at two analyzing windows labeled as  $2i$  and  $2i+1$ . Consider  $D^{(2i)} = \{\psi_k^{(2i)}\}_{k=1, \dots, N_c}$  and  $D^{(2i+1)} = \{\psi_k^{(2i+1)}\}_{k=1, \dots, N_c}$  to be the sets of phase functions provided by the WHAF for the  $2i$ -th and the  $(2i+1)$ th windows, respectively. Using these phase functions, we build the sets of time-frequency filters  $\{W_k^{(2i)}\}_{k=1, \dots, N_c}$  and  $\{W_k^{(2i+1)}\}_{k=1, \dots, N_c}$ . When applied to the received signal,  $x(t)$ , these filters provide  $N_c$  output signals for each window, i.e.,

$$\begin{aligned} \{s_k^{(2i)}\} &= \{W_k^{(2i)} x(t)\}_{k=1, \dots, N_c} \\ \{s_k^{(2i+1)}\} &= \{W_k^{(2i+1)} x(t)\}_{k=1, \dots, N_c} \end{aligned} \quad (5)$$

Using these filtered samples, we decide that two phase functions,  $\psi_m^{(2i)}$  and  $\psi_n^{(2i+1)}$ , be regrouped (i.e., they belong to the same time-frequency component) if the correlation of corresponding samples,  $\{s_m^{(2i)}\}$  and  $\{s_n^{(2i+1)}\}$ ,  $m, n = 1, \dots, N_c$ , is maximal for all pairs  $(m, n)$ :

$$\begin{aligned} (\hat{m}, \hat{n}) &= \arg \max_{\substack{m \in [1, N_c] \\ n \in [1, N_c]}} \langle s_m^{(i)}(t), s_n^{(i)}(t) \rangle \\ \Rightarrow \psi_m^{(1)} \circ \psi_n^{(2)} &\subset \text{trajectory of signal } x(t) \text{ over } [(i-1)T, (i+1)T] \end{aligned} \quad (6)$$

where “ $\circ$ ” symbolizes the fusion of two phase functions belonging to the same trajectory occupying the time interval  $[(i-1)T, (i+1)T]$ . This trajectory, denoted by  $l$ , most appropriately characterizes the collective Doppler behavior of the multipath component. This is typically the strongest signal, which is the middle component of the filtered Doppler

trajectories.

After covering all segments of the signal, we define the time-frequency trajectory corresponding to the captured signal component as the fusion of phase functions:

$$\phi_l(t) = \psi_{k_1}^{(1)} \circ \psi_{k_2}^{(2)} \circ \dots \circ \psi_{k_N}^{(N)} \quad (7)$$

where  $N$  is the number of analyzing windows and  $k_i$  is the index of the phase function obtained from the  $i$ th window.

### C. Stationarization

Once a coarse estimate of the phase law of one of the signal components of the maneuvering target is obtained, the signal frequency signature can be stationarized as following:

$$y(t) = x(t) \exp(-j\phi_l(t)), \quad (8)$$

Note that the conversion should reserve the frequency separation between the three different Doppler signatures.

### D. Spectrum Estimation

With signals being stationarized, all the three components are approximately stationary and are distributed around the low-frequency region. Therefore, a number of parametric and nonparametric spectral analysis methods can be applied for frequency estimation. In this paper, the short-time Fourier transform is used.

## V. PROCESSING RESULTS

### A. Doppler Signature Estimation

The tracking result of the above method for the measured OTHR signal is illustrated in Fig. 5. The coarse estimation is done by using windows of 560 samples, half overlapped. For each window, the second order WHAF is applied and the estimation of the chirp's parameters is performed. As evident in this figure, the tracking is accurate and that the global time-frequency behavior is properly estimated. The estimated trajectory is used to stationarize its content. This is the main difference with respect to the method considered in [4]. Whereas the time-frequency trajectory in [4] was used to extract the corresponding signal's component (by global time-frequency filter), in this paper, we use this trajectory merely to stationarize the time-frequency content of the signal. In so doing, we avoid the inherent tracking errors that could lead to an inaccurate component extraction.

Using the coarse Doppler estimation illustrated in Fig. 5, the spectrogram of the stationarized signal  $y(t)$  of eq. (8) is plotted in Fig. 6. The window size is 2048 samples (51.2 seconds). We can observe that the time-frequency content of this signal is almost stationary, and the three components can be clearly distinguished over most of the observation period. This allows us to use a short-time spectral estimation technique to provide improved local frequency estimation. At this point, the physical modeling is inferred. For each sliding window, three spectral peaks are estimated which constitute the spectrum vectors of the three components. The results are shown in Fig. 7. From these results, the elevation Doppler

frequency is estimated as one half of the difference between the Doppler frequencies of the 1st and the 2nd components. The result is shown in Fig. 8 together with the Doppler frequency obtained from the GPS positions.

After the frequencies of the stationarized signal are estimated, we can apply the inverse frequency law to obtain an estimation of the instantaneous Doppler frequencies of the three OTHR Doppler signal components. Fig. 9 shows the estimated Doppler frequencies of the three components, depicted in red circles. The results well coincide with the spectrogram and the estimated Doppler frequencies based on the GPS positions, which are also shown in the same figure.

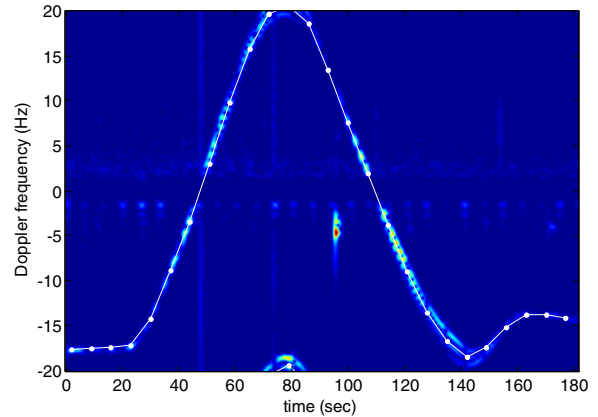


Figure 5. Coarse estimation of the Doppler signature.

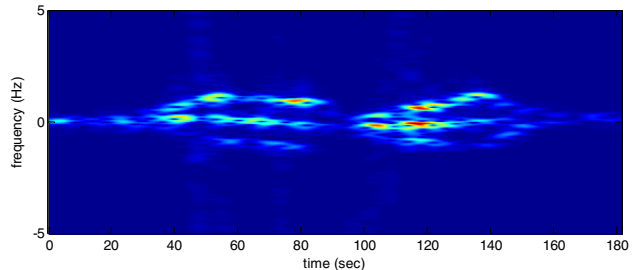


Figure 6. Spectrogram of the stationarized signal.

### B. Target Altitude Tracking

The elevation velocity of the target can be estimated from the Doppler estimates, given that the estimates of the ionosphere altitude and the slant range are available. The relationship between the Doppler frequency and the target velocity depicted in eq. (2), is rather simplified owing to the flat-earth ionosphere mirror model assumption. To obtain more accurate results for the underlying problem, the elevation velocity and, consequently, the relative altitude of the target are estimated numerically based on the spherical geometry model. We first compute the sensitivity of Doppler frequency with respect to a unit change of the target altitude over the time period of one second, and the estimated Doppler signature is compared to the sensitivity measure so that the actual target altitude can be estimated. Fig. 10 shows the estimated result of the target's relative altitude based on the Doppler estimates depicted in Fig. 8. It is clear that the

estimated altitude results reveal all the maneuvering details of the target's descending over the entire observation period with a very small difference to the ground truth recorded at the GPS receiver.

### VI. CONCLUDING REMARKS

In this paper, we have introduced a novel time-frequency analysis method in the context of the OTHR signals. The estimation of the instantaneous Doppler frequency laws corresponding to multipath associated with a maneuvering target provides useful information about the trajectory of the target, especially its vertical motion. The stationarization of time-varying multi-component Doppler signatures into fixed frequency sinusoidal components was performed and considered key to providing accurate target Doppler signature estimations. The superior performance of the proposed technique is demonstrated using real data measured by an Australian OTHR system.

### REFERENCES

- [1] R. H. Anderson, S. Kraut, and J. L. Krolik, "Robust altitude estimation for over-the-horizon radar using a state-space multipath fading model," *IEEE Trans. Aerospace Electron. Syst.*, vol. 39, no. 1, pp. 192-201, Jan. 2003.
- [2] Y. Zhang, M. G. Amin, and G. J. Frazer, "High-resolution time-frequency distributions for manoeuvring target detection in over-the-horizon radars", *IEE Proc.-Radar Sonar Navig.*, vol. 150, no. 4, pp. 299-304, Aug. 2003.
- [3] L. Cohen, *Time-frequency Analysis*, Prentice Hall, 1995.
- [4] C. Ioana, M. G. Amin, Y. D. Zhang, and F. Ahmad, "Characterization of Doppler effects in the context of over-the-horizon radar," *IEEE Radar Conference*, Washington D.C., May 2010.
- [5] C. Ioana and A. Quinquis, "Time-frequency analysis using warped-based high-order phase modeling," *EURASIP J. Applied Signal Processing*, vol. 2005, no. 17, pp. 2856-2873, Sept. 2005.

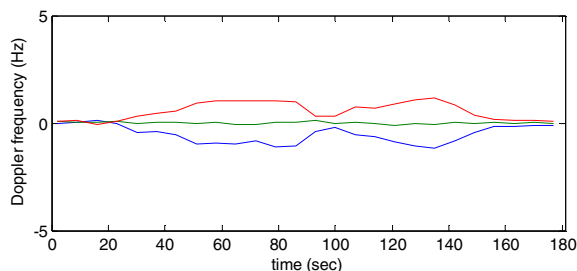


Figure 7. Estimated Doppler frequencies of the stationarized signal.

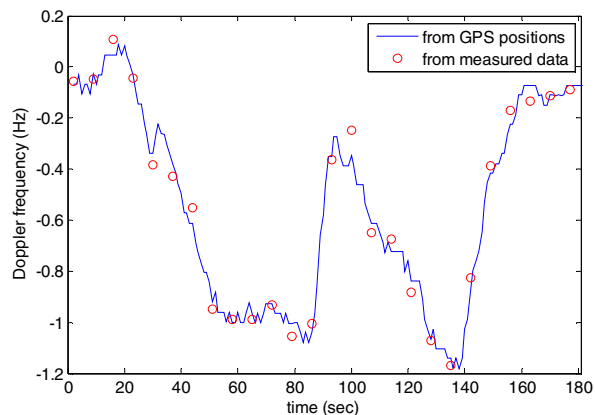


Figure 8. Estimated elevation Doppler frequencies.

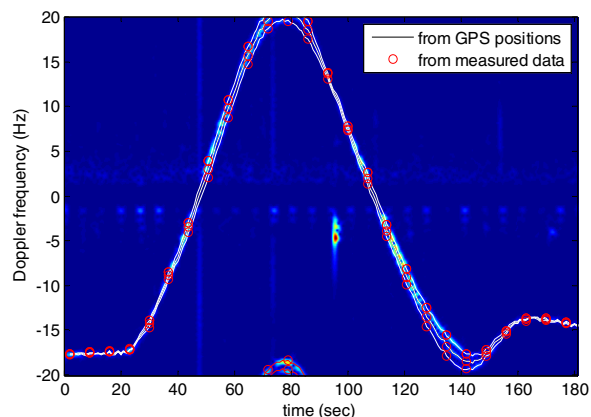


Figure 9. Estimated instantaneous Doppler frequency laws.

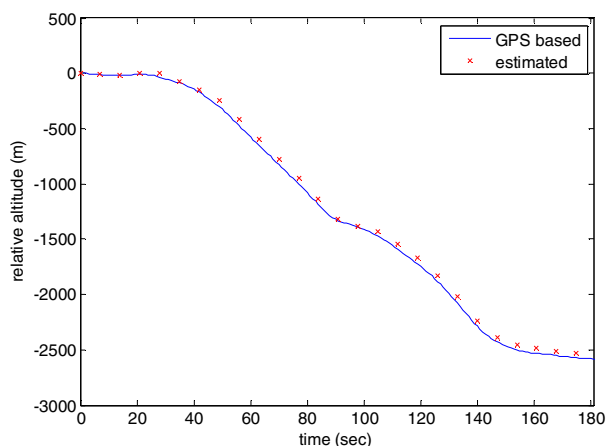


Figure 10. Estimated relative target altitude.